NMR Imaging of Pulp Suspension Flowing through an Abrupt Pipe Expansion

Darren F. Arola and Robert L. Powell
Dept. of Chemical Engineering and Materials Science, University of California, Davis, CA 95616

Michael J. McCarthy
Dept. of Food Science and Technology, University of California, Davis, CA 95616

Tie-Qiang Li
Dept. of Radiology, Lucas MRS Center, Stanford University, Stanford, CA 94305

Lars Ödberg
AssiDoman AB, 105 22 Stockholm, Sweden

Nuclear magnetic resonance imaging was used to measure velocity profiles of water and an aqueous, 0.5 wt. % (consistency) wood pulp suspension flowing through a circular pipe in the vicinity of a 1:1.7 tubular expansion. Flow images are provided for various flow rates and axial positions with respect to the expansion plane. For water, both laminar and turbulent flows were investigated. Pulp suspension flows were investigated upstream and downstream from the expansion plane. The expansion plane imparts shear layer instabilities that disrupt the fiber floc network. The fiber reflocculation length is proportional to the bulk flow rate. We determined a mean reflocculation time of approximately 510 ms for this pulp fiber consistency.

Introduction

Fluid flow through an axisymmetric expansion is of interest from both the practical and theoretical perspectives. Abrupt pipe expansions are found in equipment such as mixing vessels and heat exchangers. A specific case where the design of expansion units is crucial to equipment performance is in the paper machine headbox. Grammage uniformity, one of the most important paper properties for all paper grades (Ilmoniemi et al., 1986), is directly influenced by the headbox nozzle and the cross-flow distributor, both of which incorporate expansions in their designs. To provide insight into the physics of such flows, we have studied the flow of an aqueous, wood-pulp suspension through an abrupt, axisymmetric pipe expansion. Of particular interest was the effect of the expansion upon the pulp fiber network at different volumetric flow rates. Our objectives included obtaining upstream and downstream velocity profiles, determining the effect of the wall shear stress in the vicinity of the expansion on the structure of the pulp fiber network, and measuring the mean reflocculation time.

The axisymmetric expansion has been studied as an example of a captive annular eddy (Macagno and Hung, 1967) and a detached wall-bounded shear layer (Iribarne et al., 1972; Back and Roschke, 1972; Acrivos and Schrader, 1982; Latornell and Pollard, 1986). Two parameters of particular interest are the inlet Reynolds number at which the maximum reattachment length occurs and the critical Reynolds number for the onset of shear-layer instability. There is general agreement that for a Newtonian fluid, at low upstream Reynolds numbers, the shear-layer reattachment length increases linearly, or nearly so, with the inlet Reynolds number. Past a critical upstream Reynolds number of approximately 635, the reattachment length is found to decrease (Latornell and Pollard, 1986). In the early experiments, which used the same fluids, different results were found for the relationship between the inlet Reynolds number and the reattachment length. Subsequently, it was suggested that these inconsistencies resulted from different upstream conditions (Back and

Correspondence concerning this article should be addressed to D. F. Arola.
Present address of D. F. Arola: MBA Polymers, Inc., 500 West Ohio Avenue, Richmond, CA 94804.

Roschke, 1976). Most recently, Latornell and Pollard (1986) demonstrated that the onset of shear-layer instabilities as well as the reattachment length were dependent upon the inlet velocity profile. If the inlet conditions are turbulent and plug flow is observed, the maximum reattachment length occurs at an upstream Reynolds number less than 635 (Latornell and Pollard, 1986). Non-Newtonian fluids exhibit shear-layer reattachment and vortex lengths that differ from Newtonian fluids. Existing numerical (Perera and Walters, 1977; Nakamura and Sawada, 1990) and experimental results (Pak et al., 1990; Townsend and Walters, 1994) indicate that the reattachment and vortex lengths decrease with fluid elasticity in the laminar flow regime. In the turbulent flow regime, the reattachment length for a viscoelastic fluid was found to be two or three times greater than that observed for water, whereas a purely viscous non-Newtonian fluid provided results similar to water in both flow regimes (Pak et al., 1990). Castro and Pinho (1995) found that elongational elastic effects may only arise under turbulent flow conditions, and emphasized the importance of accurately characterizing the elastic behavior of non-Newtonian fluids in turbulent flow. Through numerical analysis non-Newtonian fluids that exhibit yield values have been found to produce reattachment lengths that are less than those found for Newtonian fluids. This inverse relationship between yield stress and reattachment length holds throughout the laminar flow regime (Vradis and Otugen, 1997). It has been experimentally shown that a non-Newtonian glass fiber suspension has larger vortex lengths than a Newtonian fluid for Reynolds numbers less than 12 (Townsend and Walters, 1994).

Our objective is to apply a noninvasive flow measurement technique, nuclear magnetic resonance imaging (NMRI), to the study of flow through an expansion. Other flow measurement techniques include those that photograph or track the movement of tracer particles within the fluid medium, measure disturbances produced by impact probes or anemometers immersed in the fluid, or utilize the optical behavior of fluids (Emrich, 1981). It is also possible to measure the voltages and current conditions on the physical boundaries encompassing the fluid to determine the spatial distribution of conductivity or permittivity within the region of interest (Plaskowski et al., 1995). Few techniques, however, are able to provide precise and accurate measurement over a wide range of conditions noninvasively without the need to add tracer particles. Even fewer are able to obtain quantitative measurements using optically opaque systems, such as aqueous pulp suspensions at fiber concentrations used in papermaking. The combination of broad fiber size distribution and high concentration limits the success of laser Doppler anemometry and light reflection techniques due to the fiber fines that provide large secondary scattering surfaces (Ek et al., 1978). Most impact probes and light-guide probes suffer from bad resolution, interference of the fibers with the probe openings, and often cause flow disturbances (Ek et al., 1978). NMRI has been successful in noninvasively measuring pipe flows of aqueous wood pulp suspensions (Seymour et al., 1993; Li et al., 1994a,b, 1995c), through an abrupt contraction (Li et al., 1994c, 1995a) and a continuous conical contraction (Li et al., 1995b) at fiber consistencies from 0.5–0.92% such as those commonly encountered in headboxes of conventional paper machines. For these fiber concentrations, the ^{1}H NMR signal from the fibers is negligible, and the flow measurements are based upon the suspending fluid. NMRI has previously been used to study the flow of water through an abrupt expansion (Xia et al., 1992), although aqueous pulp suspensions at a consistency of 0.5% exhibit complex rheological behavior and the flows of such suspensions are qualitatively different from those of water.

Our work focused on the dynamics of fiber flocs as they pass through an abrupt expansion and on changes in the velocity profiles upstream and downstream of the expansion. Except in its immediate vicinity, the expansion plane was found to have no effect upon the upstream floc network or velocity profile. Downstream from the expansion plane, however, the pulp suspension exhibited different levels of fluidization, or fiber disentanglement in the suspending medium, that were dependent upon the inlet bulk flow. Fiber fluidization increased as the bulk flow increased, which was indicated by both the intensity distribution and shape of the NMR velocity profile images. The distance downstream from the expansion plane that was required for the fibers to reflocculate and form a plug network was found to be proportional to the inlet bulk flow.

Pulp Suspension Flow Characteristics

Aqueous pulp suspensions exhibit non-Newtonian fluid behavior. This is due to the ability of the fibers to impart elasticity and strength to the mixture. Under shear flow, fibers collide by rotation and translation and form flocs by mechanical entanglement. Depending on the fiber physical properties such as aspect ratio, shear modulus, and fiber surface chemistry, above a critical fiber concentration flocs tend to form a continuous network structure throughout the suspension. For the pulp fibers used in our experiments individual flocs form at about 0.05 wt. %, and at a fiber concentration greater than 0.4 wt. % the individual flocs form a continuous network that changes the fluid properties dramatically. Deformation of the fiber microstructure during flow depends on the relationship between the applied stresses and the interparticle colloidal and mechanical interlocking forces (Li et al., 1994b). The relationship between the applied stress and microstructure of the pulp suspension remains poorly understood because of the chemical and physical complexity of the pulp suspension and the difficulty in devising experiments in which direct observation of the structure and fluid dynamics can be made. Depending on the fiber properties and the flow conditions, all or part of the floc and network structure in the suspension can be disrupted and a "fluidized" state created (Li et al., 1994b). In this case, fluidization signifies fibers that are free of mechanical entanglement.

There are three pipe flow categories encountered as the flow rate is increased for pulp suspensions: plug flow, mixed flow, and turbulent flow (Forgacs et al., 1958). At the lowest flow rates, plug flow exists if there is no movement of fibers relative to one another and the velocity gradient is confined to a fiber-free water layer near the pipe wall. A network of individual fiber flocs composes the plug. Mixed flow arises at higher flow rates if the velocity gradient at the wall (or turbulent stresses) is large enough to cause the disruption of the plug network near the pipe wall, which liberates fibers or flow. Turbulent flow exists at the highest flow rates if the intense

small-scale fluid motions are able to disperse the floc network and individual flocs on a continuous basis.

A completely dispersed fiber suspension is defined as one where every fiber is free of mechanical entanglement. This does not necessarily mean that the fibers do not interact, only that if they do, the interaction is transmitted through the suspending medium (Wahren, 1979). Suspensions with higher pulp consistencies require larger turbulent stresses to disrupt the fiber flocs, as indicated by estimates of the power requirements needed for pulp-suspension fluidization (Bennington and Kerekes, 1996). Increasing consistency in unit operations is attractive in industry, because it diminishes the volume of suspending medium and ultimately reduces production costs.

In practice, fluidized suspensions exist only when there is a continuous supply of energy that inhibits floc reformation. Turbulence is not synonymous with full dynamic equilibrium between flocculation and dispersion, and indeed, in decaying turbulent fields, coherent flocs are likely to form. Such a flow can consist of a region of high turbulence leading up to an obstruction, downstream from which there is decreasing turbulence. These can occur downstream from pumps, rectifier rolls in headboxes, as well as in pipes leading from well-agitated reservoirs, valves, and expansions (Kerekes et al., 1985). There are a number of studies concerning the reflocculation process in decaying turbulence (Bonano, 1984; Kerekes et al., 1985; Francis and Kerekes, 1992). Attention has been paid to the reflocculation time, which is the time needed for the disrupted fibers to reflocculate upon entering decaying turbulent conditions (Kerekes et al., 1985).

Flow Imaging

The NMR measurement procedure used in this study yields spatially resolved fluid displacements by combining a displacement-sensitive pulsed-gradient spin echo (PGSE) (Karger and Heink, 1983; Kose et al., 1985; Callaghan et al., 1988; Xia and Callaghan, 1990; Callaghan, 1991; Frydman et al., 1993; Arola et al., 1997, 1998) with a one-dimensional imaging technique that spatially resolves these displacements. The imaging technique relies upon a spin echo to form the signal and the application of a gradient transverse to the direction of flow during its acquisition. In a Cartesian coordinate system, the z-direction, which is parallel to the magnet bore, is the flow axis while x and y are perpendicular to flow. A frequency-selective 90° radio-frequency (RF) pulse, combined with an applied G_z gradient, excites a plane of spins perpendicular to the direction of flow. Following excitation, the spins experience a spatially dependent phase shift produced by the first G_z gradient pulse, which is subsequently inverted by a 180° RF pulse. The second G_z gradient pulse imposes a phase proportional to the final position. The net phase from the two gradient pulses is proportional to the distance traveled in the z-direction during the time interval between the G_z gradient pulses, which we will refer to as the flow time, or T. Each G_z pulsed-gradient step produces an independent observation of the fluid displacement over T. Applying a gradient transverse to the flow axis during signal acquisition provides the spatial resolution. The experiment is then repeated with G_z varying in equal increments from positive to negative.

The time-domain signal for our imaging sequence is given by

$$S(k_x, q_z; T) = \int \left[\rho(x) \exp(i2\pi k_x x) \times \int P(\Delta z, x; T) \exp(i2\pi q_z \Delta z)\, d\Delta z \right] dx. \quad (1)$$

We have used x in Eq. 1 to denote that the transverse imaging gradient applied upon signal acquisition is G_x, although G_y would be equally possible. A two-dimensional Fourier transform with respect to q_z and k produces a map of $P(\Delta z, x; T)\rho(x)$ for each transverse position x, where $P(\Delta z, x; T)$ is the conditional probability density that a fluid element at position x will displace Δz within the pulse sequence time interval T, while $\rho(x)$ is the position-dependent spin number density. The reciprocal space variables k_x and q_z are the conjugate variables of position x and displacement Δz, respectively. The variable k_x is given by $(2\pi)^{-1}\gamma G_x t$, where γ is gyromagnetic ratio of nuclei (rad/s·Gauss), G_x is the imaging gradient magnitude and t is the signal acquisition dwell time. The variable q_z is given by $(2\pi)^{-1}\gamma G_z \tau$, where G_z is the pulsed gradient magnitude and τ is the duration of the pulsed gradient.

The intensity distribution of the displacement profile resulting from the two-dimensional Fourier transform of the time-domain signal in Eq. 1 is the projection of the full three-dimensional displacement profile onto a two-dimensional Cartesian plane (Arola et al., 1998). The projection occurs along the dimension perpendicular to that of the imaging gradient, G_x, and the signal intensity along the imaging dimension is a projection of the sample density onto the x-axis given by

$$\rho_y(x) = \int_{-\infty}^{\infty} \rho(x, y)\, dy, \quad (2)$$

where the subscript y denotes a projection along the y-axis. Although theoretically the integration is over the infinite domain, in practice we need only consider the integration over the spatial extent of the sample within the NMR probe.

The resulting fluid-displacement profile is represented by a ridge of intensity on an intensity-displacement-position plot. There is also extraneous intensity from the projection operation and noise. Thresholding the intensity to a level 10% of maximum removes the extraneous intensity resulting from the noise. However, a higher thresholding level is needed to compensate for the intensity resulting from the projection operation, which does not represent the displacement profile. Thresholding levels set at 30% of full scale are generally sufficient in removing all of the extraneous intensity without adversely affecting the displacement profile. Velocity and position values are assigned to the discrete intensities composing the image. With this analysis, it is difficult to distinguish the transverse position x in the tube from a velocity profile measured with respect to radial coordinates and x is replaced by r to simplify the discussion of our results.

If each G_z pulsed-gradient step of the NMR experimental timing diagram is not observing the same displacement value for the fluid element, the resulting image reflects Fourier

transform artefacts, which arise when processing the time-domain signal in Eq. 1. When such effects are large, these artefacts make the velocity profile ridge indiscernible from the base-line noise. Fluid motions resulting from turbulence and unsteady flow are the main cause of displacement variations over the flow time, T. By repeating each pulsed-gradient step and coadding the measured signals, it is possible to create an ensemble average of the fluid displacement value. Coadding signals, in most imaging applications, improves the image signal-to-noise ratio (S/N) when there are low levels of nuclei for each imaging volume element. Here, signal coadding is performed due to the displacement variation of the fluid volume element over the observation time. When the fluid-element displacement observation times are long compared to the displacement fluctuation time scale attributed to turbulent flow, an improved NMR signal is observed and the increased S/N ratio of the reconstructed image allows the velocity profile to be determined (Li et al., 1995c). If the number of coadditions is NA, the total fluid flow observation time is $NA * T$.

Analysis of the intensity distribution of the time-averaged image under turbulent flow conditions provides information about the local turbulence intensity. It has been shown that the relative image intensity is directly related to the local turbulence intensity in water (Li et al., 1994d). This has more recently been applied to pulp-suspension flow under pipe flow conditions where the resultant intensity distribution of the velocity profile with and without increased observation times has been related to dispersion and reflocculation (Li et al., 1995c). Images that display turbulence (low signal intensity) on a short time scale or using few signal coadditions may show plug-flow regions with increasing observation times. This indicates that in turbulent flow the fiber flocs may undergo a reversible dispersion and reflocculation process (Li et al., 1995c). The number of signal coadditions needed to produce the plug core reflects the characteristic time for the pulp reflocculation process. If increasing the observation time is unable to yield steady plug cores, the disruption of the fiber flocs is considered predominant, causing the flocs in the suspension to be transient and the fibers essentially fully dispersed.

Materials and Methods

The closed flow-loop system consisted of polyvinyl chloride (PVC) piping with 3.1 m of straight piping upstream from the 1:1.7 abrupt expansion (15.3 mm to 26.2 mm) to provide fully developed flow (length/diameter ≅ 200). A positive displacement pump (SPS-20 Sine pump, Orange, USA) was used. A series of measurements was obtained at different axial positions in the vicinity of the expansion for each flow rate. Figure 1 shows a cross-sectional view of the abrupt expansion.

The 0.5 wt. % fiber suspension was composed of fully bleached hardwood (birch) kraft pulp (Södra Skogsägarna, Mörrum, Sweden) with an average size of approximately 1 mm in length and 0.040 mm in diameter, providing an aspect ratio of 25. Fiber suspensions of this type and consistency provide a yield value that is difficult to quantify using a controlled stress rheometer with vane and cup geometry (Weldon, 1995). Based upon yield value measurements of this fiber type at consistencies of 0.75 and greater, we estimated the yield

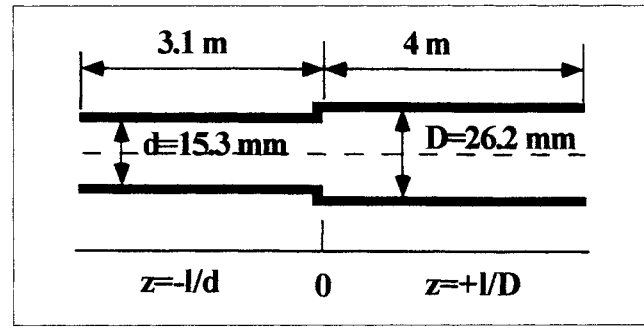

Figure 1. Cross-sectional view of the abrupt pipe expansion.

The expansion plane is the axial position origin.

value of the suspension used in this work to be less than 0.5 Pa. The suspending medium for the fibers was distilled water doped with $CuSO_4$. Copper ions provide paramagnetic relaxation centers in the fluid that efficiently decrease the NMR spin-lattice relaxation time of the ^1H spins, allowing for decreased experimental times.

The NMR velocity profiles were obtained using a General Electric CSI-II NMR imaging spectrometer connected to a 2.0-Tesla Oxford superconducting magnet (corresponding to 85.5-MHz ^1H resonance frequency). The horizontally oriented magnet has a clear inner bore diameter of 300 mm. A set of unshielded gradient coils produce three orthogonal gradients G_x, G_y, and G_z driven by an Oxford-2339 water-cooled gradient power amplifier where G_z is parallel to the magnet bore. The maximum gradient amplitude for all three gradients is approximately 0.2 Gauss/mm.

For all velocity profiles the field of view (FOV) perpendicular to displacement was 50 mm with 128 divisions (or samples) yielding a resolution of approximately 390 μm. The FOV parallel to velocity was changed according to the fluid flow rate. The resolution of the velocity profiles ranged from 1.2 mm/s to 9.4 mm/s with 128 samples. The mean fluid flow rate was measured using timed fluid collections. Since the NMR signal is directly proportional to the number of nuclear spins within a volume element, the image slice thickness was changed to improve the S/N ratio. The slice thickness ranged from 3 mm to 10 mm, but was typically 5 mm. The NMR pulse sequence employed a two-step phase cycle to eliminate base-line artefacts. This made the number of signal coadditions for each pulsed-gradient value at least two. Signal coadding beyond this amount was performed near the region of the expansion and at the higher flow rates. The total experimental time varied from less than 2 min with two $NA = 2$ to a few hours with $NA = 200$. Table 1 presents the image-slice thickness, NA, observation time, axial position relative to the expansion plane expressed in pipe diameters, approximate water upstream Reynolds number, approximate downstream water Reynolds number, and the velocity resolution of the images obtained for this study. We note that we do not characterize the flow conditions for pulp suspensions using a Reynolds number. The complex behavior of these materials makes such a characterization difficult, and, instead, we use mean flow conditions to characterize the flow.

Table 1. Main NMRI Experimental Parameters and Reynolds Numbers for the Experiments with Water

Image/Velocity Data	Slice Thickness (mm)	*NA*	Observed Time (ms)	Axial Position (Pipe Dia.)	Approx. Upstream *Re* No.	Approx. Downstream *Re* No.	Velocity Resolution (mm/s)
2A	5	2	14	−61.2	1,870	1,090	3.9
2B	3	2	14	0.0	1,870	1,090	3.9
2C	10	16	115	0.0	1,870	1,090	3.9
2D	3	2	14	0.8	1,870	1,090	3.9
2E	3	16	115	1.5	1,870	1,090	3.9
2F	5	16	115	3.1	1,870	1,090	3.9
2G	5	16	165	8.9	1,870	1,090	2.3
2H	5	2	21	10.8	1,870	1,090	2.3
2I	5	2	21	22.5	1,870	1,090	2.3
3A	5	16	230	1.1	430	250	1.2
3B	5	16	165	1.1	1,060	620	2.3
3C	5	16	115	1.1	1,390	810	3.9
4A	5	2	21	10.8	1,060	620	2.3
4B	5	16	168	10.8	1,590	930	2.3
4C	5	2	21	10.8	2,360	1,380	2.3
5A	5	2	7	−3.3			7.8
5B	5	2	7	−3.3			7.8
5C	5	200	1,740	−3.3			9.4
6A	5	8	72	0.8			7.8
6B	5	2	18	0.8			7.8
7A	5	2	21	9.6			3.9
7B	5	2	21	9.6			3.9
7C	5	16	168	9.6			3.9

Results and Discussion

Water

For the presentation of our results, the expansion plane is set at $z = 0$. Axial positions are described using the number of upstream or downstream pipe diameters from the expansion plane, with the upstream axial positions taken as negative. Figure 2 displays NMR velocity profile images for water at various cross sections upstream and downstream of the abrupt expansion. The upstream Reynolds number was approximately 1,870. This corresponds to a downstream Reynolds number of approximately 1,090. Parabolic velocity profiles were found on both sides of the expansion plane, Figures 2A and 2I at axial positions −61.2 and 22.5, respectively. For all figures, Table 1 gives the details of the experimental conditions used for each measurement, including the actual axial location.

Figure 3 shows velocity data taken 1.1 pipe diameters from the expansion plane at three bulk flow rates with corresponding downstream Reynolds numbers of approximately 250, 620, and 810, respectively. Secondary flow was observed for all three flow rates with the maximum retrograde velocities being 9.6 mm/s, 6.9 mm/s, and 7.8 mm/s, respectively. The similar velocity magnitudes in the recirculation zone suggested that increasing the bulk flow does not have a large effect upon the velocity of the recirculating fluid immediately downstream from the expansion plane and near the tube wall. Our observation of a recirculating zone is consistent with earlier NMR imaging studies of water flow through an abrupt expansion (Xia et al., 1992).

Figure 4 provides NMR velocity profile images at 10.8 pipe diameters. For these measurements, the downstream Reynolds numbers were approximately 620, 930, and 1,380. As the bulk flow rate increased, we observed the onset of flow instability that was indicated by both the shape and intensity distribution of the velocity profile. For each flow rate, the velocity profile deviated further from parabolic shape. Comparing Figures 4A and 4C, respectively, there is an apparent decrease in the intensity approaching the tube center for the higher bulk flow rate even though the NMR experimental parameters were identical for each measurement. As discussed by Li et al. (1994d), the apparent decrease in the intensity near the tube center with the increase in the Reynolds number reflects small-scale velocity fluctuations associated with turbulent flow. Observations further downstream, at the point where relaminarization should occur, were not made.

Pulp suspension

Figure 5 provides three flow images for a 0.5% consistency pulp suspension −3.3 pipe diameters from the expansion plane. In this experiment, the flow rate was increased, providing upstream plug velocities from approximately 190 mm/s to 1,100 mm/s. The velocity gradient of Figure 5A is confined to a small layer near the pipe wall, whereas the data in Figure 5B show velocity variations over a larger radial extent than those in Figure 5A. Furthermore, a comparison of the intensity distribution of Figures 5A and 5B for these two bulk flows with identical NMR experimental parameters shows that the plug diameter has decreased by approximately 35% with the increase in bulk flow. These observations coincide with the definition for plug and mixed flow (Forgacs et al., 1958) and hence, Figure 5A shows a plug region in the center, whereas Figure 5B demonstrates mixed flow. The image in Figure 5C was generally of low intensity and showed Fourier

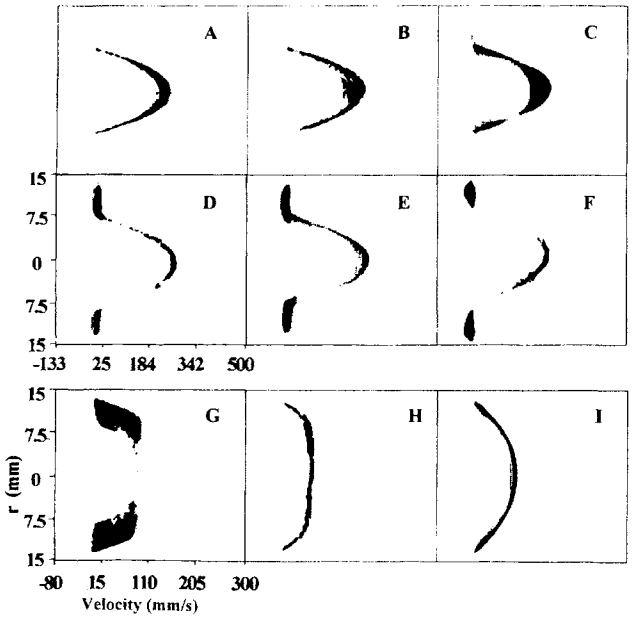

Figure 2. Velocity profile images of water at a flow rate corresponding to an upstream Reynolds number of 1,870 and a downstream Reynolds number of 1,090.

The upstream to downstream progression of images for a total of seven axial positions starts at −61.2 and ends at 22.5 (Table 1). The axial positions are reported as upstream and downstream pipe diameters, respectively. Parabolic velocity profiles are apparent at axial positions of −61.2 and 22.5.

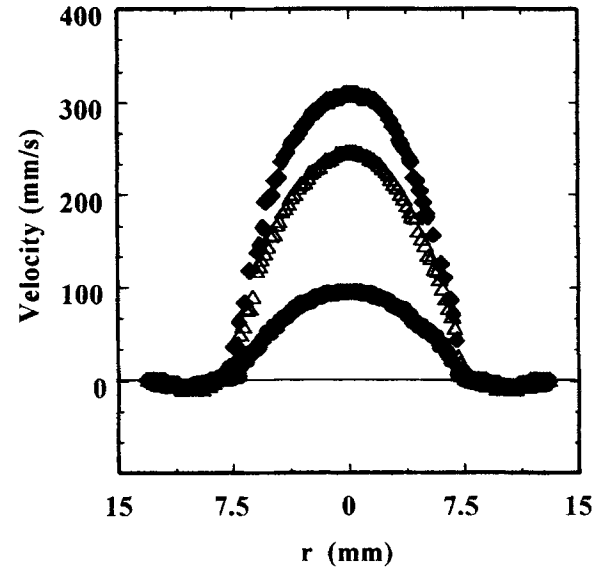

Figure 3. Effect of increasing bulk flow on velocity for water flowing through an expansion at an axial position of 1.1 at downstream Reynolds numbers of 250 (●), 620 (△), and 810 (◆).

As the flow rate was increased, negative velocity values were found, indicating the presence of secondary flow.

transform artefacts with an observation time of 7 ms, but it was possible to determine a plug core when the observation time was increased to 1,740 ms. As discussed by Li et al. (1995c), the low intensity at a short time scale and the appearance of a plug-flow region with increased observation time indicates a reversible dispersion and reflocculation process. The increase in observation time was established by increasing the number of NMR signal acquisitions, or *NA*. Furthermore, the low-intensity region between the plug core, making up approximately 50% of the pipe diameter, and the pipe wall revealed a fully fluidized region.

Figure 6 displays two velocity profile images at 0.8 pipe diameters downstream from the expansion plane. The plug velocities were approximately 230 mm/s and 340 mm/s, respectively. The plug diameter decreased by approximately 17% as the bulk flow was increased. The observation times for these velocity profiles were 72 ms and 18 ms, respectively. The velocity resolution for these measurements prevented quantitative analysis of the presence of recirculating fluid near the downstream tube wall, although Figure 6 displays intensity in this region. However, both images of Figure 6 demonstrated a fluidized region between the center plug core and the pipe wall. Unlike the velocity profiles for water at nearly the same axial position, the velocity profiles for the fiber suspension exhibited a large velocity gradient as seen by the abrupt change in velocity. The emerging pulp flow from the upstream pipe behaved like a well-defined jet that was unable to rapidly increase in size as the cross section of the pipe expanded. The upstream flow approaching the expansion plane was separated from the suspension near the pipe wall immediately downstream from the expansion. This resulted in a separation zone with a large velocity gradient and flow deceleration. The flow separation dispersed the fiber network structure, as demonstrated by the intensity distribution of the image.

Our fiber suspension results qualitatively agree with the flow characteristics observed for a glass fiber suspension (Townsend and Walters, 1994). The strong vortex activity, relative to a Newtonian fluid, results in a separation zone with a large velocity gradient. The glass fibers had an aspect ratio of 80, nearly three times that for our cellulose fibers. These were suspended in a Newtonian fluid with a viscosity of 1 Pa·s at a concentration of 0.025%. Our pulp suspension bulk flow rates are an order of magnitude higher than those in the glass fiber suspension study, disallowing a quantitative comparison of our results.

Because of the qualitative nature of the observations made here, as well as those by Bennington and Kerekes (1996) and Forgacs et al. (1958), it is not inconsistent to look to the Bingham model to provide insight into the observed behavior. This comes at some risk. Even in pipe flow, while the Bingham model may capture the plug behavior in the tube center, it does not address the important mechanisms at work outside the plug region where unsteady flow occurs. Likewise, the dynamics of the microstructure is not linked to the prediction of the model. Still, for a qualitative comparison we can consider the flow of Bingham fluids in expansion geometries, which have determined that the yield value decreases the reattachment length (Vradis and Ötugen, 1997). The type and consistency of pulp used in this study prevented accurate measurement of the yield value using a controlled stress rheometer with vane and cup geometry, although we can

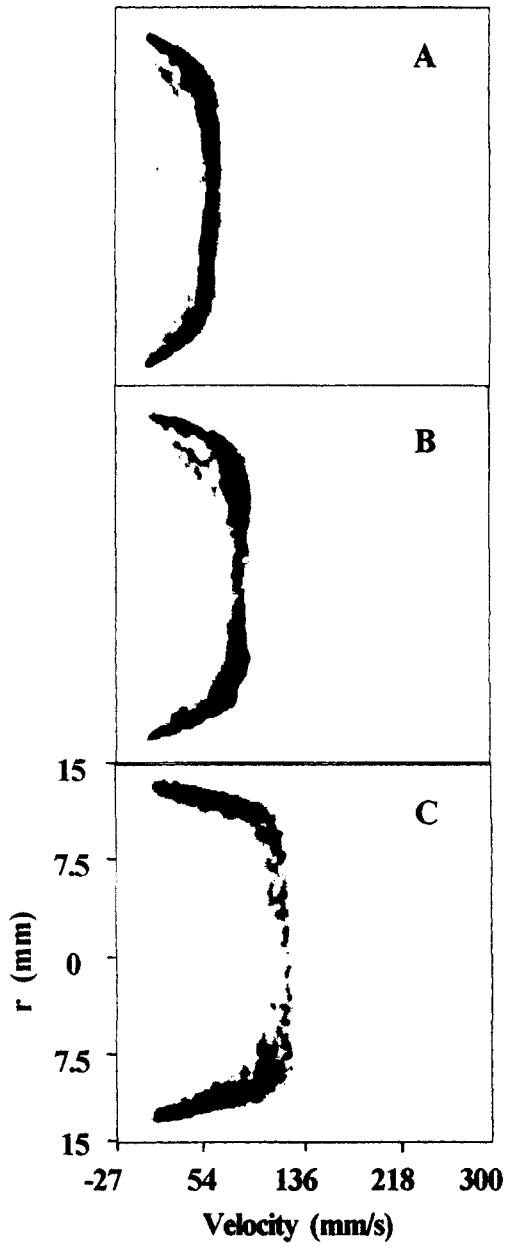

Figure 4. Effect of increasing bulk flow rate on velocity profile images of water at 10.8 pipe diameters downstream.

The downstream Reynolds numbers are 620 (A), 930 (B), and 1,380 (C). The change in shape of the velocity profiles and the intensity decrease near the tube center of the tube with increasing *Re* demonstrate the ability of the abrupt expansion to destabilize the flow.

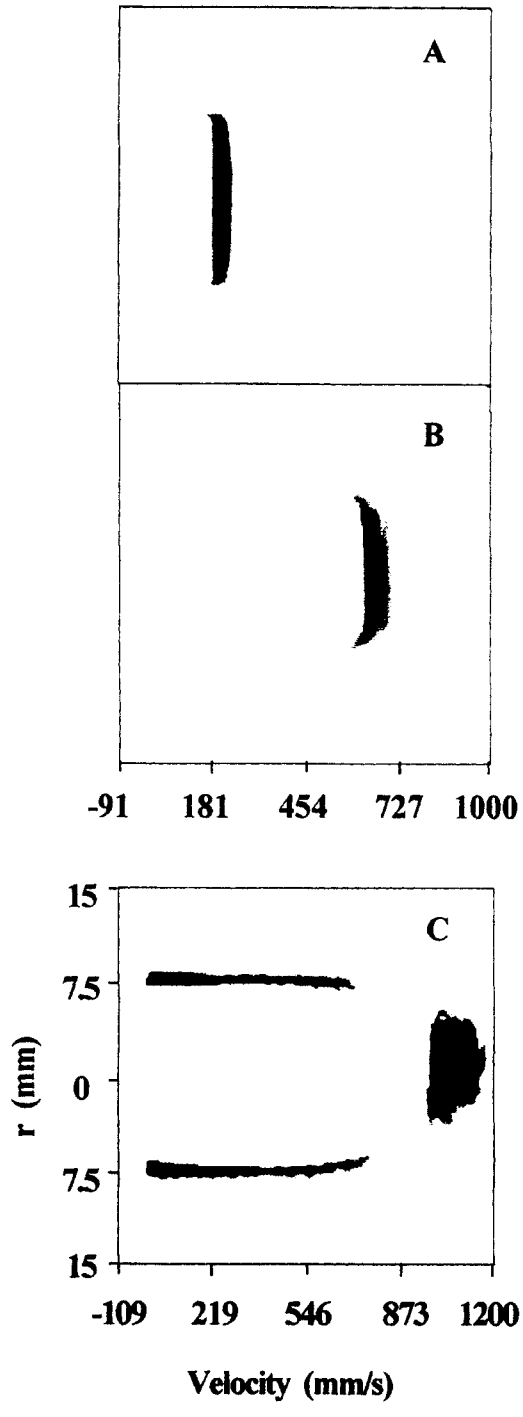

Figure 5. Effect of increasing bulk flow rate on the velocity profiles of a pulp suspension at $z = -3.3$.

Figures 5A and 5B display plug and mixed flow, respectively, determined by the decrease in plug diameter and the increase of the axial velocity gadient near the tube wall. For the image of Figure 5C, the NMR fluid flow observation time was increased to 1,740 ms to produce the velocity profile. Fourier transform artefacts dominated the image at an observation time of 7 ms. A fully fluidized region was found for Figure 5C. This is the low-intensity region between the plug core and tube wall. The plug core width decreased with increasing bulk flow rate indicating improved fiber floc disruption. The plug diameter for the largest bulk flow is 50% of the tube diameter.

speculate that it was less than 0.5 Pa (Weldon, 1995). Although we did not directly measure reattachment lengths in this work, the strong vortex activity and separation zone suggest a reattachment length greater than that observed for water, and this would conflict with the numerical studies of Vradis and Ötugen (1997). This discrepancy may result from two factors. First, the bulk flow rates involved in this work are larger than the numerical studies and, indeed, small-scale fluctuations are likely to occur, negating the steady flow as-

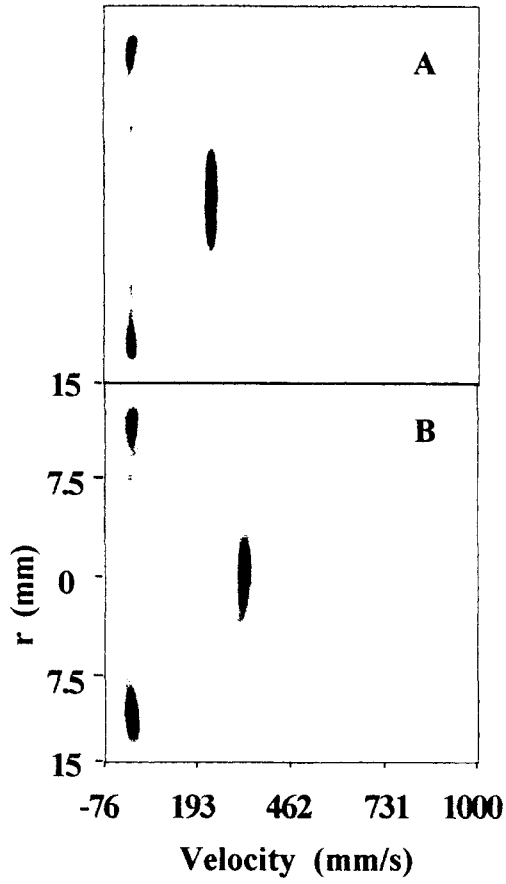

Figure 6. Effect of increasing bulk flow rate on the velocity profile of a pulp suspension at $z = 0.8$.

Both profiles clearly display large velocity gradients and unsteady flow between the plug core and region near the pipe wall, as indicated by the low signal intensity. Comparing the two velocity profiles, the plug diameter has decreased by 17% with the increase in flow rate.

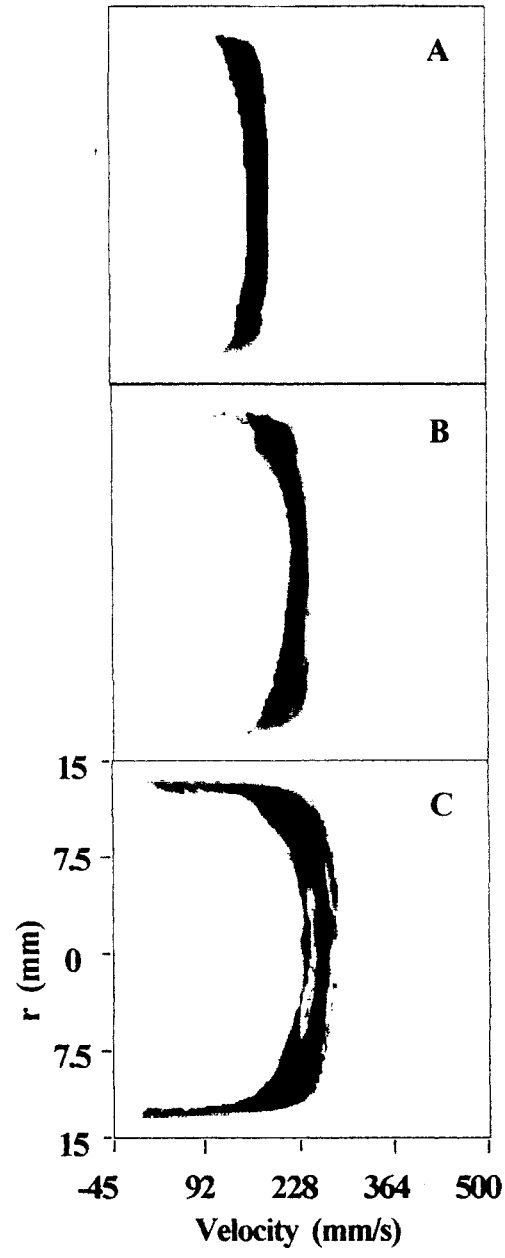

Figure 7. Effect of increasing bulk flow rate on the velocity profile for a pulp suspension at $z = 9.6$.

These velocity profiles demonstrate varying degrees of mixed flow as denoted by the intensity distribution and shape of the NMR velocity profile. As the bulk flow rate increases, the velocity profiles exhibit less plug-flow behavior with an increase in the radial extent of the velocity gradient. The plug velocities are approximately 170 mm/s (A), 220 mm/s (B), and 260 mm/s (C).

sumption. Second, the fiber suspension, as mentioned earlier, cannot be considered an ideal Bingham fluid with the dynamics of the microstructure playing an important role.

Figure 7 displays three NMR velocity profile images 9.6 pipe diameters from the expansion plane, with plug velocities of approximately 170 mm/s, 220 mm/s, and 260 mm/s. Figure 7C required an observation time of 168 ms, eight times greater than Figures 7A and 7B, to produce a velocity profile image. Comparing Figure 7A with the upstream velocity profile of Figure 5A, where the plug velocities are 170 mm/s and 190 mm/s, respectively, the downstream velocity profile exhibited mixed flow, whereas the upstream velocity profile exhibited plug flow. This disparity in the intensity distribution for the two velocity profiles reaffirmed the observations based upon the data in Figure 6 that the expansion geometry aids in the dispersion of the cellulose fibers.

Our final objective in this study was to determine the relation between the bulk flow rate and the reflocculation of the pulp fibers downstream from the expansion plane. The data of Figure 8 present the axial distance downstream from the expansion plane at which increased observation times were not needed to produce a discernible velocity profile for a given mean flow rate. The ability to attain a velocity profile with a short observation time indicated that the fibers and flocs were forming a coherent structure. Each data point displays the axial position where a minimum observation time of approximately 15 ms could produce a velocity profile image at a given bulk flow rate. If the bulk flow rate was increased while maintaining the 15-ms observation time at the recorded axial position, the velocity profile image was dominated by Fourier

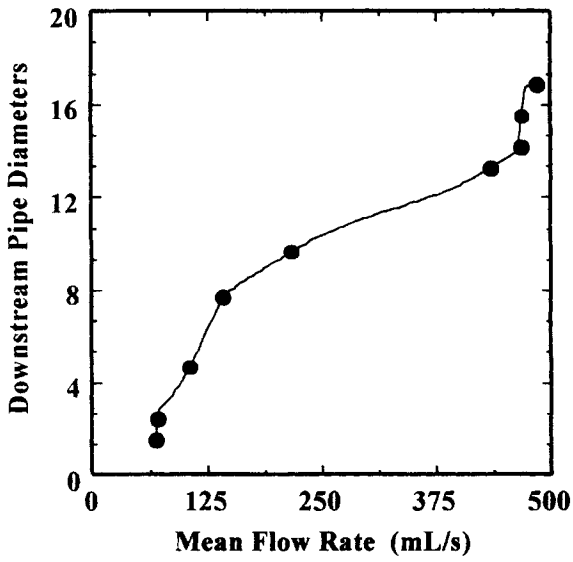

Figure 8. Downstream axial position (—●—) vs. threshold mean flow rate for the pulp suspension under decaying turbulence flow conditions.

Flow rates greater than the plotted values at each position require NMR observation times greater than 15 ms to achieve an image not dominated by Fourier transform artefacts. Hence, these positions represent the length of pipe needed for the disrupted pulp suspension to form coherent structures that exhibit mixed flow characteristics.

transform artefacts that indicated that the fibers and flocs were experiencing a reversible dispersion and reflocculation process along with the small-scale velocity fluctuations associated with turbulence. The mean flow rate was calculated using the average of timed fluid collections. The flocculation time estimate for each bulk flow was calculated from the data of Figure 8 by dividing the axial position by its corresponding average velocity. The average velocity was approximated by dividing the volumetric flow rate by the pipe cross-sectional area. The mean reflocculation time estimate was found by fitting the reflocculation length vs. average velocity data to a straight line and was found to be 510 ms with a standard deviation of 140 ms. Our estimate of the mean reflocculation time was of the same order as those tabulated by Kerekes and coworkers (Kerekes et al., 1985). Table 2 provides a summary of prior work with regard to the reflocculation time for a number of different pulp-suspension studies involving decaying turbulence, and the table compares those results to the value obtained by the present study.

Table 2. Reflocculation Time of Pulp Suspensions Under Decaying Turbulence Flow Conditions*

Investigators	Consistency (wt. %)	Flow Velocity (mm/s)	Reflocculation Time (ms)
Parker	0.155	760–1,040	< 2,000
Kallmes	0.5	Not provided	500
	1.0		1,000
	2.0		40
	3.0		10
	4.0		1
Grundström et al.	3.0	Not provided	2–10
	4.0		1
d'Incau	0.45	125–2,000	160
Takeuchi et al.	0.14–0.86	830	500–1,500
Bonano	1.0	7,600	7
		9,100	14
		10,200	12
	2.0	9,100	14
		10,200	12
Kerekes et al.	0.3	1,300	840
This work	0.5	130–900	510 ± 140

*Our reflocculation time estimate of 510 ms is in close agreement with the results of Kallmes (1997) at a consistency of 0.5%.

Conclusions

The flow field downstream from the abrupt expansion plane for the pulp suspension exhibited behavior similar to that of a confined jet. The flow-separation region downstream from the expansion plane is highly effective in disrupting fiber flocs. We are able to characterize the flow instability and fluidization of the fiber network by analyzing both the intensity distribution and shape of the NMR velocity profiles as a function of the downstream position and the NMR observation time. Our findings on the reflocculation time are in good agreement with prior work involving pulp-suspension flow of decaying turbulence.

Acknowledgments

This work was supported by grants from the U.S. Department of Agriculture NRI Competitive Grants Program/USDA 92-37103-7946 and the Swedish Pulp Industry's Foundation for Technical and Forestry Research and Education.

Literature Cited

Acrivos, A., and M. L. Schrader, "Steady Flow in a Sudden Expansion at High Reynolds Numbers," *Phys. Fluids*, **25**, 923 (1982).

Arola, D. F., G. A. Barrall, R. L. Powell, K. L. McCarthy, and M. J. McCarthy, "Use of Nuclear Magnetic Resonance Imaging as a Viscometer for Process Monitoring," *Chem. Eng. Sci.*, **52**, 2049 (1997).

Arola, D. F., G. A. Barrall, R. L. Powell, and M. J. McCarthy, "Measurement Time Reducing Methods of NMR Flow Profile Imaging: Hankel Transforms, Velocity Aliasing and Rapid Repetition Time," *JMRA*, **3**, 175 (1997).

Back, L. H., and E. J. Roschke, "Shear-Layer Flow Regimes and Wave Instabilities and Reattachment Lengths Downstream of an Abrupt Circular Channel Expansion," *J. Appl. Mech.*, **39**, 677 (1972).

Back, L. H., and E. J. Roschke, "Technical Note: The Influence of Upstream Conditions on Flow Reattachment Lengths Downstream of an Abrupt Circular Channel Expansion," *J. Biomech.*, **9**, 481 (1976).

Bennington, C. P. J., and R. J. Kerekes, "Power Requirements for Pulp Separation Fluidization," *TAPPI J.*, **79**, 253 (1996).

Bonano, E. J., "A Study of Floc Breakup and Formation in Flowing Concentrated Fiber Suspensions," *Int. J. Multiphase Flow*, **10**, 623 (1984).

Callaghan, P. T., C. D. Eccles, and Y. Xia, "Rapid Communication NMR Microscopy of Dynamic Displacements: k-Space and q-Space Imaging," *J. Phys. E: Sci. Instrum.*, **21**, 820 (1988).

Callaghan, P. T., *Principles of Nuclear Magnetic Resonance Microscopy*, Clarendon Press, Oxford (1991).

Castro, O. S., and F. T. Pinho, "Turbulent Expansion Flow of Low Molecular Weight Shear-Thinning Solutions," *Exp. Fluids*, **20**, 42 (1995).

d'Incau, S., *Proc. TAPPI Eng. Conf.*, TAPPI Press, Atlanta, p. 583 (1983).
Ek, R., K. Moller, and B. Norman, "Simultaneous Measurement of Velocity and Concentration in Fiber Suspension Flow," *Proc. Dynamic Flow Conf.*, I.M.S.T., Marseille, p. 745 (1978).
Emrich, R. J., *Methods of Experimental Physics*, Vol. 18, *Fluid Mechanics*, Academic Press, New York (1981).
Forgacs, O. L., A. A. Robertson, and S. G. Mason, "The Hydrodynamic Behavior of Paper-Making Fibres," *Pulp Paper Mag. Can.*, **59**, 117 (1958).
Francis, D. W., and R. J. Kerekes, "Flow and Mixing Behavior of Low- and Medium-Consistency Fiber Suspensions Downstream of a Valve," *TAPPI J.*, **75**, 113 (1992).
Frydman, L., J. S. Harwood, D. N. Garnier, and G. C. Chingas, "Position-Displacement Correlations in Fluids from Magnetic Resonance Gradient-Echo Shapes," *J. Magn. Reson. Ser. A*, **101**, 240 (1993).
Grundström, K.-J., B. Norman, and D. Wahren, "High Consistency Forming of Paper," *TAPPI*, **56**, 81 (1973).
Ilmoniemi, E., L. Aroviita, and E. Yli-kokko, "The Role of Headbox Turbulence Generators in Grammage Uniformity," *Appita*, **39**, 35 (1986).
Iribarne, A., F. Frantisak, R. L. Hummel, and J. W. Smith, "An Experimental Study of Instabilities and Other Flow Properties of a Laminar Pipe Jet," *AIChE J.*, **18**(4), 689 (1972).
Kallmes, O., "Flocculation of Pulp Suspensions," *Paper Trade J.*, **161**, 44 (1977).
Karger, J., and W. Heink, "The Propagator Representation of Molecular Transport in Microporous Crystallites," *J. Magn. Reson.*, **51**, 1 (1983).
Kerekes, R. J., R. M. Soszynski, and P. A. Tam Doo, "The Flocculation of Pulp Fibers," *Papermaking Raw Materials*, Vol. 1, V. Punton, ed., Mechanical Engineering Publications, London, p. 265 (1985).
Kose, K., K. Satoh, T. Inouye, and H. Yasuoka, "NMR Flow Imaging," *J. Phys. Soc. Japan*, **54**, 81 (1985).
Latornell, D. J., and A. Pollard, "Some Observations on the Evolution of Shear Layer Instabilities in Laminar Flow Through Axisymmetric Sudden Expansions," *Phys. Fluids*, **29**, 2828 (1986).
Li, T.-Q., R. L. Powell, L. Ödberg, M. J. McCarthy, and K. L. McCarthy, "Velocity Measurements of Fiber Suspensions in Pipe Flow by the Nuclear Magnetic Resonance Imaging Method," *TAPPI J.*, **77**, 145 (1994a).
Li, T.-Q., J. D. Seymour, R. L. Powell, M. J. McCarthy, K. L. McCarthy, and L. Ödberg, "Visualization of Flow Patterns of Cellulose Fiber Suspensions by NMR Imaging," *AIChE J.*, **40**, 1408 (1994b).
Li, T.-Q., R. L. Powell, M. J. McCarthy, and L. Ödberg, "Axisymmetric Entry Flow of Wood Pulp Suspension Investigated by Means of Nuclear Magnetic Resonance Imaging," *Proceedings of the 1994 Engineering Conference*, TAPPI Press, Atlanta, p. 735 (1994c).
Li, T.-Q., J. D. Seymour, R. L. Powell, K. L. McCarthy, L. Ödberg, and M. J. McCarthy, "Turbulent Pipe Flow Studied by Time-Averaged NMR Imaging Measurements of Velocity Profile and Turbulent Intensity," *Magn. Reson. Imaging*, **12**, 923 (1994d).
Li, T.-Q., L. Ödberg, R. L. Powell, M. Weldon, and M. J. McCarthy, "Flow of Pulp Suspension through an Abrupt Contraction Studied by Flow Encoded Nuclear Magnetic Resonance Imaging," *Nordic Pulp Paper Res. J.*, **10**, 133 (1995a).
Li, T.-Q., R. L. Powell, and M. J. McCarthy, "Flow of Pulp Suspensions Through a 4:1 Continuous Conical Contraction Studied by NMR Imaging Technique," *Proceedings of 1995 Engineering Conference*, TAPPI Press, Atlanta, p. 209 (1995b).
Li, T.-Q., M. Weldon, L. Ödberg, M. J. McCarthy, and R. L. Powell, "Pipe Flow Behavior of Hardwood Pulp Suspensions Studied by NMRI," *J. Pulp Paper Sci.*, **21**, J408 (1995c).
Macagno, E., and T. K. Hung, "Computational and Experimental Study of a Captive Annular Eddy," *J. Fluid Mech.*, **28**, 43 (1967).
Nakamura, M., and T. Sawada, "Numerical Study of the Unsteady Flow of Non-Newtonian Fluid," *ASME J. Biomech. Eng.*, **112**, 100 (1990).
Pak, B., Y. I. Cho, and S. U. S. Choi, "Separation and Reattachment of Non-Newtonian Fluid Flows in a Sudden Expansion Pipe," *J. Non-Newtonian Fluid Mech.*, **37**, 175 (1990).
Parker, J. D., "Velocity Profile Measurements for Pulp Suspensions," *TAPPI J.*, **55**, 162A (1961).
Perera, M. G. N., and K. Walters, "Long Range Memory Effects in Flows Involving Abrupt Changes in Geometry, Part 2: The Expansion/Contraction/Expansion Problem," *J. Non-Newtonian Fluid Mech.*, **2**, 191 (1977).
Plaskowski, A., M. S. Beck, R. Thorn, and T. Kyakowski, *Imaging Industrial Flows*, Institute of Physics Publishing, London (1995).
Seymour, J. D., J. E. Maneval, K. L. McCarthy, M. J. McCarthy, and R. L. Powell, "NMR Velocity Phase Encoded Measurements of Fibrous Suspensions," *Phys. Fluid A*, **5**, 3010 (1993).
Takeuchi, N., S. Senda, K. Namba, and G. Kuwabara, "Pulp Suspension Refloculation Times," *APPITA*, **37**, 223 (1983).
Townsend, P., and K. Walters, "Expansion Flows of Non-Newtonian Liquids," *Chem. Eng. Sci.*, **49**, 749 (1994).
Vradis, G. C., and M. V. Ötugen, "The Axisymmetric Sudden Expansion Flow of a Non-Newtonian Viscoplastic Fluid," *J. Fluids Eng.*, **119**, 193 (1997).
Wahren, D., "Fiber Network Structures in Papermaking Operations," *Proceedings 1979 Cutting Edge Conference*, Inst. Paper Chem., Appleton, WI, p. 112 (1979).
Weldon, M. S., "Pipe Flow of Pulp Suspensions Examined by Nuclear Magnetic Resonance Imaging," MS Thesis, Univ. of California, Davis (1995).
Xia, Y., and P. T. Callaghan, "The Measurement of Diffusion and Flow in Polymer Solutions Using Dynamic NMR Microscopy," *Makromol. Chem. Macromol. Symp.*, **34**, 277 (1990).
Xia, Y., P. T. Callaghan, and K. R. Jeffrey, "Imaging Velocity Profiles: Flow Through an Abrupt Contraction and Expansion," *AIChE J.*, **38**, 1408 (1992).

Manuscript received Dec. 16, 1997, and revision received Oct. 5, 1998.